Journal of Alloys and Compounds, 176 (1991) 269–283
JAL 0018

Age-hardening characteristics in an AuCu–14at.%Ag alloy

Kunihiro Hisatsune and Koh-Ichi Udoh
Department of Dental Materials Science, Nagasaki University School of Dentistry, 7-1 Sakamoto-machi, Nagasaki (Japan)

Bambag Irawan Sosrosoedirdjo
Department of Dental Materials, Faculty of Dentistry, University of Indonesia, Salemba 4, Jakarta (Indonesia)

Toshihiko Tani and Katsuhiro Yasuda
Department of Dental Materials Science, Nagasaki University School of Dentistry, 7-1 Sakamoto-machi, Nagasaki (Japan)

(Received April 22, 1991)

Abstract

Age-hardening characteristics and associated phase transformations were studied by electrical resistivity, hardness tests, X-ray and electron diffraction, transmission electron microscopy and scanning electron microscopy observations in an AuCu–14at.%Ag pseudobinary alloy. The critical temperature of ordering was determined to be 650 K and the spinodal temperature was estimated to be 640 K. Age hardening at 623 K was attributed to nucleation and growth processes of the AuCu II′ metastable ordered phase even though the aging temperature was just below the spinodal temperature. While hardening in the lower temperature range took place at two stages, the former was due to spinodal decomposition and the latter was brought about by ordering of AuCu I′ and/or AuCu II′ metastable phases depending on aging temperature. Overaging was induced by grain boundary precipitation of AuCu I and/or AuCu II ordered and silver-rich α_2 stable phases.

1. Introduction

In recent years phase transformation in commercial dental gold alloys has been studied considerably to elucidate the age-hardening mechanism [1–6]. However, explication of the mechanisms of age hardening in commercial dental gold alloys is very difficult, because the alloys have an extremely complex combination of constituents, frequently containing five or more constituents. Therefore, it is necessary to study age-hardening characteristics and the associated phase transformation in Au–Cu–Ag ternary alloys, since commercial dental gold alloys are composed of gold, copper and silver as essential constituents.

It has been known that the Au–Cu–Ag ternary system exhibits three distinguishable phase changes in certain composition regions, *i.e.* ordering based on AuCu or Cu_3Au, precipitation induced by a nucleation and growth

0925-8388/91/$3.50

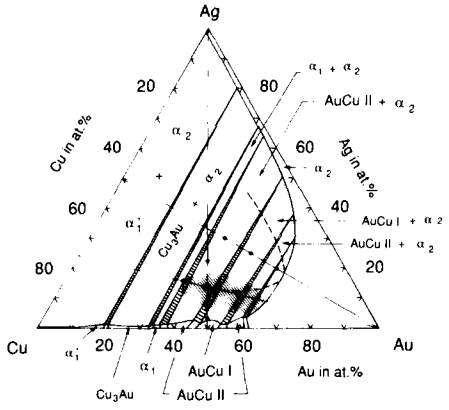

Fig. 1. Isothermal section of a plausible phase diagram of the Au–Cu–Ag ternary system at 573 K.

mechanism and spinodal decomposition. It is also well known that these phase changes bring about a significant age hardening in the alloys depending on their composition, especially on the atomic ratio of gold and copper, with appropriate heat treatment.

Figure 1 shows an isothermal section at 573 K of the plausible Au–Cu–Ag ternary phase diagram which was constructed by superimposing the theoretical phase diagram calculated using the cluster variation method by Yamauchi *et al.* [7] on experimental data [8–14]. In the phase diagram, the dots show the composition of the experimental alloys which were examined mainly using transmission electron microscopy (TEM) and selected area electron diffraction (SAED) as well as X-ray diffraction (XRD) techniques. The double circle exhibits the composition of the alloy used in the present study. The full lines correspond to the miscibility gap of two-phase decomposition and the three-phase triangles. The spinodal locus of $\partial^2 G/\partial C^2 = 0$ (G, free energy; C, composition of solute) is supposed to be located at the position shown as a broken line. The shaded area indicates the composition region corresponding to commercial dental gold alloys; therefore, it is thought that the present alloy is one of a representative composition of commercial dental gold alloys.

Thus, the present study is carried out to elucidate the age hardening mechanism and characteristics in the AuCu–14at.%Ag alloy as a representative composition for commercial dental gold alloys.

2. Experimental details

The alloying constituents used in the present study had a purity of better than 99.99%. An alloy of composition Au–43at.%Cu–14at.%Ag was prepared by melting in a high frequency induction furnace. Test pieces for hardness measurements and scanning electron microscopy (SEM) examination were

cold rolled to sheets. Foils of 0.1 mm thickness were used for electrical resistivity measurements and TEM observations. Discs of 3 mm diameter were punched out from the sheet for TEM study. All test pieces were well annealed at 973 K for 1.8 ks to obtain a single-phase solid solution and then quenched into ice–brine.

Electrical resistivity was measured by a potentiometric method on a quenched thin foil specimen during continuous heating and cooling at a constant rate of 1.7×10^{-3} K s^{-1} from room temperature to the solution treatment temperature. Test pieces for hardness measurement were isothermally aged at 393, 473, 573, 623 and 673 K for various periods after solution treatment. SEM observations were made on specimens which were etched in an aqueous solution of 10% potassium cyanide and 10% ammonium persulphate after polishing by standard metallographic techniques. The discs which were aged at different temperatures for various periods of time to produce phase transformations were electrothinned to transparency by a double-jet technique in a solution of 35 g chromium trioxide in 200 ml acetic acid and 10 ml distilled water. A 200 kV electron microscope equipped with a specimen-tilting device was employed. The XRD study was carried on the powder aged specimens with nickel-filtered Cu Kα radiation.

3. Results

3.1. Electrical resistivity

An anisothermal heating and cooling excursion on a solution-treated and quenched specimen was carried out to identify temperature regions having significant changes. In Fig. 2, curve a shows resistivity changes represented by the ratio of the resistivity at a given temperature and that at the solution treatment temperature (973 K). Curve b is the associated temperature derivative

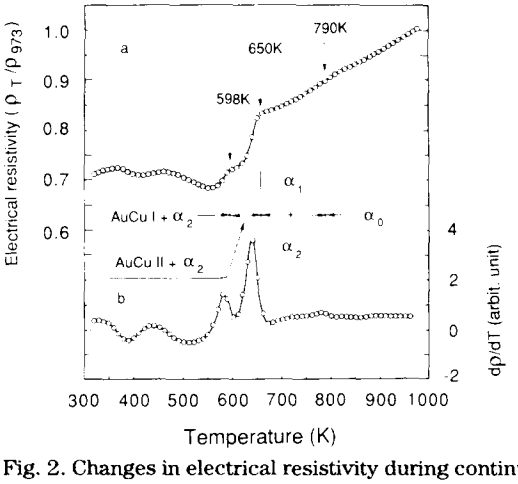

Fig. 2. Changes in electrical resistivity during continuous heating at a constant rate of 1.7×10^{-3} K s^{-1} (curve a) and its temperature derivative (curve b) plotted against temperature.

curve, $d\rho/dT$, of curve a. Here, ρ and T are electrical resistivity and temperature respectively. The heating curve of resistivity as shown in Fig. 2 yields three significant inflection points (curve a). These inflection points suggest phase transformation at 790 K, 650 K and 593 K in the alloy present. In curve b, two sharp double peaks at 580 K and 640 K and an appreciable peak at around 780 K show up. The double and neighbouring peaks are thought to be characteristics of order–disorder phase transformation and a two-phase decomposition respectively.

As seen in Fig. 2, these resistivity changes can be attributed to AuCu I (598 K), AuCu II (650 K) ordering and a two-phase decomposition (790 K) of the alloy investigated.

3.2. Age-hardening characteristics

Figure 3 shows changes in hardness during isothermal aging at various temperatures. It is obvious that predominant age hardening occurs below 623 K which is lower than the critical temperature $T_c = 650$ K for ordering. In the range 623–673 K the hardening curve exhibits an S shape which implies the occurrence of nucleation and growth processes by aging. On the contrary, the hardening curves caused by aging below 573 K represent a two-stage hardening after exhibiting a rapid increase in hardness at an early stage of aging. Thus, it is assumed that two different phase transformation processes occur in aging, associated with hardening at a temperature between 623 K and 573 K. A marked decrease in hardness, however, is found after a lengthy aging period by heterogeneous processes at the grain boundaries as will be shown later.

3.3. X-ray diffraction study

An XRD study was carried out to elucidate the sequence of phase changes associated with age hardening. Figure 4 represents changes in diffraction profiles of the 331 and 420 fundamental diffraction reflections during aging at 673 K for various periods. The solution-treated (ST) specimen, designated

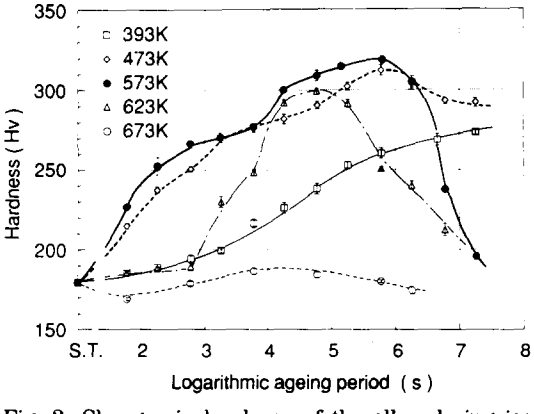

Fig. 3. Changes in hardness of the alloy during isothermal aging.

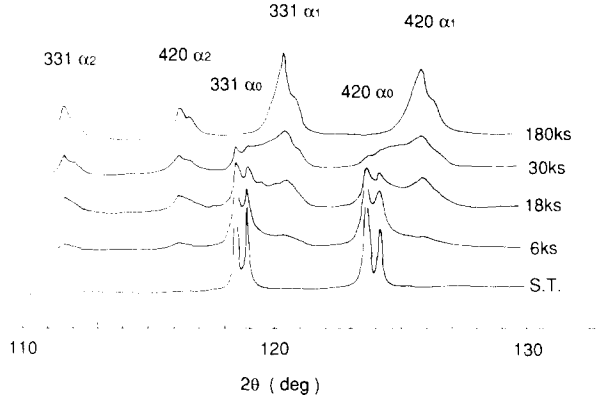

Fig. 4. Changes in X-ray diffraction profiles of the 331 and 420 fundamental reflections during aging at 673 K for various periods.

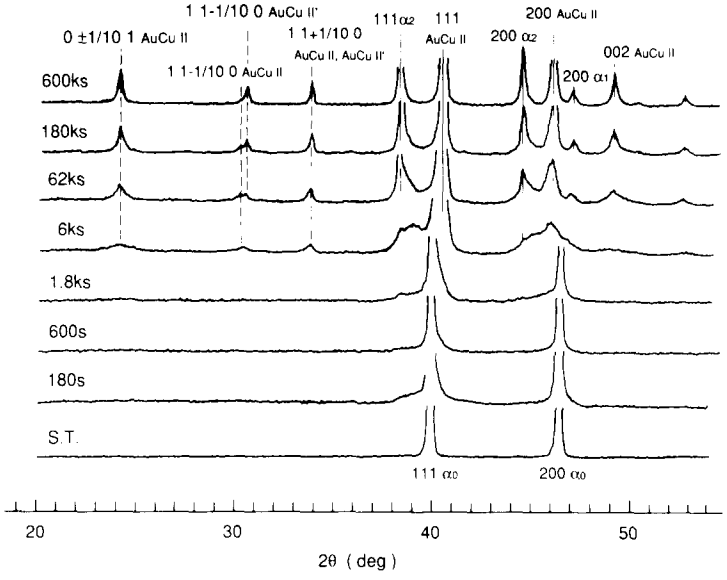

Fig. 5. Changes in X-ray diffraction profiles of superlattice reflections and fundamental reflections during aging at 623 K for various periods.

α_0, gives an f.c.c. diffraction pattern with a lattice parameter $a = 0.3907$ nm. Two sets of diffraction peaks of the 331 and 420 reflections, designated as α_1 and α_2 phases, show up in diffraction profiles during aging. Superlattice reflections and the side-bands were not observed at positions expected in the XRD pattern. The lattice parameters of the α_1 and α_2 phases were $a(\alpha_1) = 0.3897$ nm and $a(\alpha_2) = 0.4056$ nm respectively. Thus, it is suggested that a two-phase decomposition takes place during aging at 673 K.

Figure 5 shows changes in the 111 and 200 fundamental and the 001 and 110 superlattice reflections during aging at 623 K for various periods.

Superlattices formed in this temperature range are identified as metastable AuCu II′ and stable AuCu II with orthorhombic long-period superstructures. The Miller indices used here for AuCu II′ and AuCu II ordered phases are expressed as domain size $M=5$ according to Johansson and Linde [15]. Although the two-phase decomposition takes place at a relatively early stage of aging, the metastable AuCu II′ ordered phase disappears with lengthy aging. Finally, a stable AuCu II ordered phase is observed together with stable α_1 and α_2 phases. No shifts in peaks are found in the diffraction profiles for all phases generated by aging at 623 K.

Different changes in X-ray diffraction profiles show up after aging at 573 K, as seen in Fig. 6. Shifts in superlattice reflections are visible in diffraction profiles of metastable AuCu I′ with f.c.t. structure and AuCu II′ with long-period-ordered phases. This will be caused by variations in the composition of AuCu I′ and/or in the antiphase domain size of AuCu II′ phases during aging at 573 K. Furthermore, this provides evidence for the homogeneous process of phase changes in this temperature range. In Fig. 6, a heterogeneous process is also revealed in the later stage of aging. This is a sign that metastable AuCu I′ and AuCu II′ ordered phases coexist with stable AuCu I and AuCu II as well as with the α_2 phase after aging at 573 K for 6 Ms.

The metastable AuCu I′ phase was only found as an ordered phase together with α_0 phase after aging at 523 K for 300 ks. However, one must assume that the α_0 phase will change into α_1 and α_2 phases by further aging even if in this temperature range.

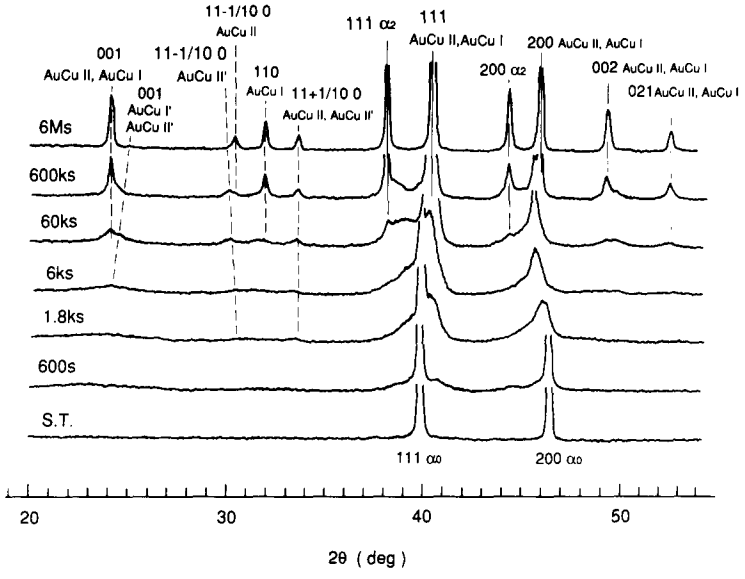

Fig. 6. Changes in X-ray diffraction profiles of superlattice reflections and fundamental reflections during aging at 573 K for various periods.

3.4. Transmission electron microscopy and selected area electron diffraction examinations

Figures 7(a) and 7(b) represent the dark field images produced by using the 200_{α_1} and 220_{α_2} reflections respectively, taken from a specimen aged at 673 K for 180 ks. An SAED pattern corresponding to the central area of Figs. 7(a) and 7(b) is shown in Fig. 7(c). The SAED pattern shows the coexistence of the α_2' phase and disordered solid solution of the α_0 phase, both f.c.c. in structure. No superlattice reflections are observed in the SAED pattern. From dark field images, it is obvious that the α_2' phase is formed on the {100} planes of the matrix α_0 phase as a plate-like precipitate by a nucleation and growth mechanism. This is because not only the characteristic satellite or side-bands in SAED patterns but also the modulated structure in TEM images were not observed at an early stage of aging.

Figure 8 shows TEM micrographs and SAED pattern taken from a specimen aged at 623 K for 100 ks. The SAED pattern shown in Fig. 8(d) indicates the formation of a metastable AuCu I′ and AuCu II′ ordered phases which are arranged with their c axes as three orientational variants X, Y and Z; for example, the Z variant means its c axis is parallel to the Z direction, *i.e.* the incident electron beam. This configuration is observed

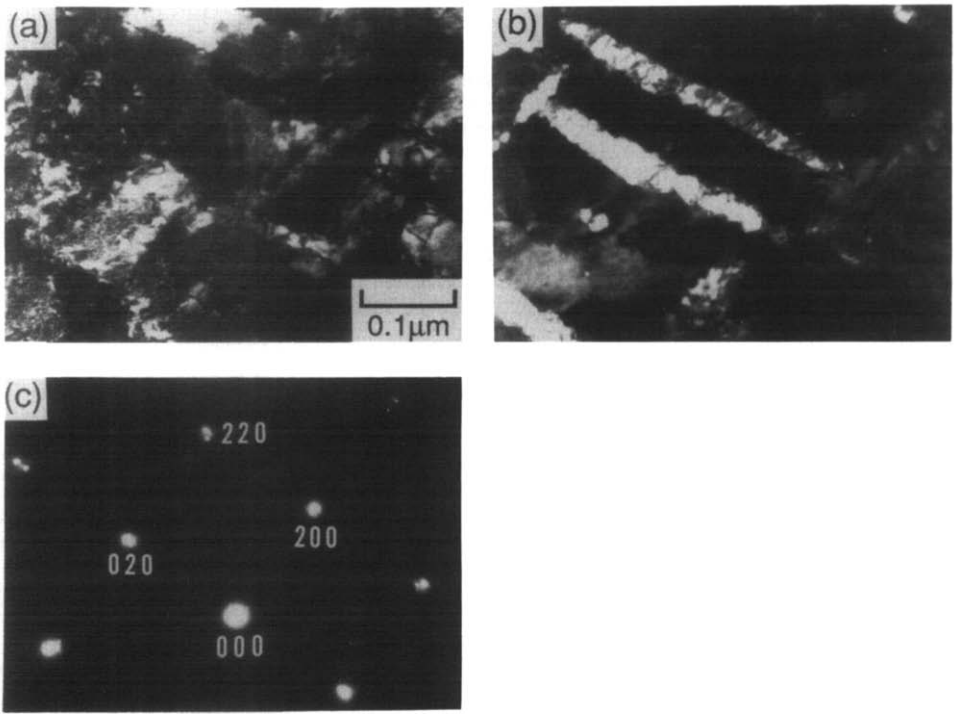

Fig. 7. TEM images and an SAED pattern taken for the specimen aged at 673 K for 180 ks; (a) the dark field image formed by using the 220_{α_1} spot; (b) the dark field image formed by using the 220_{α_2} spot; (c) SAED pattern corresponding to (a) and (b).

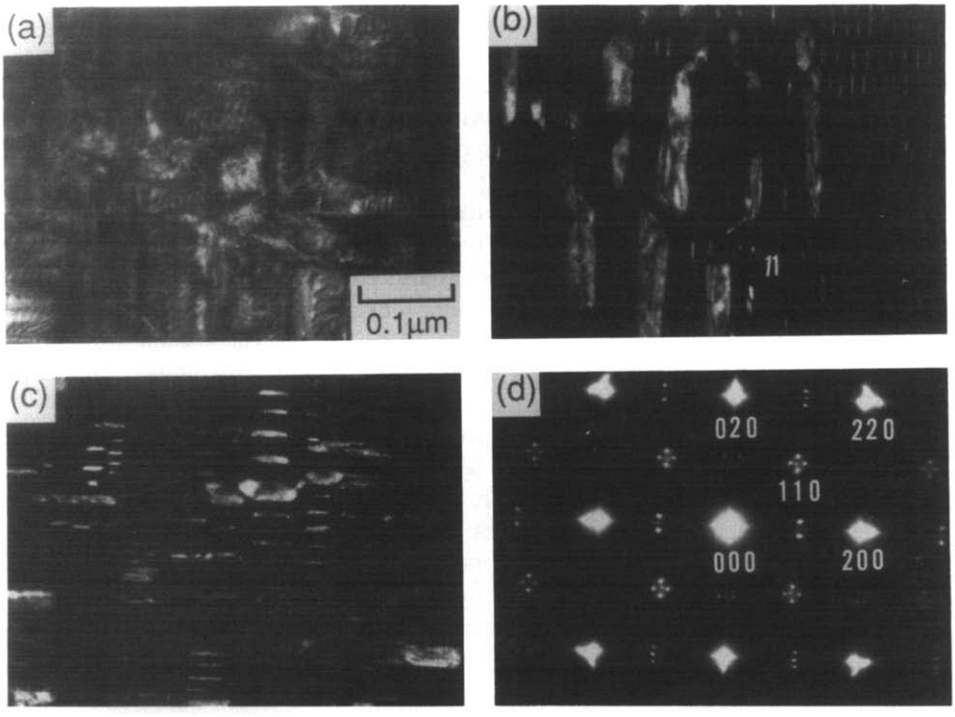

Fig. 8. TEM images and an SAED pattern taken for the specimen aged at 623 K for 100 ks: (a) the dark field image formed by using the 110 superlattice spot; (b) the dark field image formed by using the 001_X superlattice spot; (c) the dark field image formed by using the 001_Y superlattice spot; (d) SAED pattern taken from the central area of the images.

clearly in the dark field images shown in Figs. 8(a), 8(b) and 8(c). It is also clear that the ordered phases consist of thin platelets and block-like regions. The AuCu I′ ordered phase disappeared in further aging. It was therefore not a metastable ordered phase in this temperature range.

As a result of lengthy aging at 623 K, the metastable AuCu II′ ordered phase increased in size. Figure 9 exhibits TEM micrographs and an SAED pattern taken from a specimen aged at 623 K for 1 Ms. In the SAED pattern it is obvious that a metastable AuCu II′ ordered phase with three orientational variants of its c-axis is formed. Reflections from the metastable α_2' phase are also distinguishable. Because dark field images are produced from the same area, it is possible to distinguish these phases in the microstructure from each other. As seen in Figs. 9(a) and 9(b), block-like disordered α_2' fills the space between AuCu II′ ordered phase regions. In addition, thin platelets of AuCu II′ are found inside the block-like α_2'. Thus it is postulated that the block-like α_2' phase may be covered by the thin platelets of the AuCu II′ ordered phase (Fig. 9(c)). This microstructure and atomic configuration were analysed by high resolution electron microscopy, and the results will be published elsewhere [16].

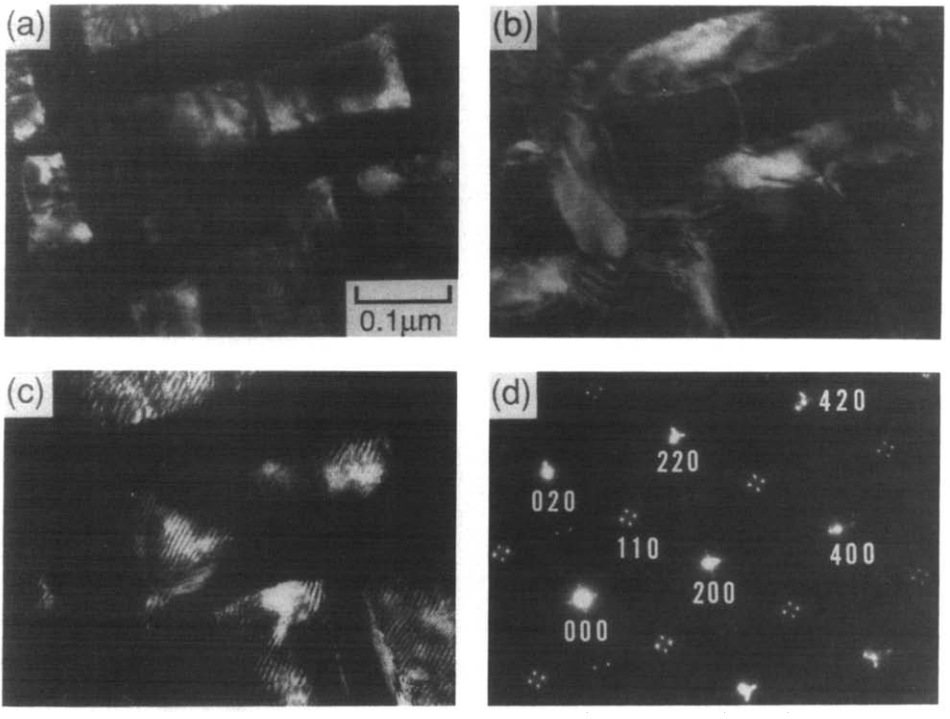

Fig. 9. TEM images and an SAED pattern taken for the specimen aged at 623 K for 1 Ms: (a) the dark field image formed by using the 220_{α_2} spot; (b) the dark field image formed by using the 220(AuCu II$'_{X,Y}$) fundamental spot; (c) the dark field image formed by using the 110(AuCu II$'_{Z}$) superlattice spot; (d) SAED pattern taken from the central area of the images.

Figure 10 shows TEM micrographs and an SAED pattern produced from a specimen aged at 573 K for 18 ks. The SAED pattern reveals the formation of the AuCu I′ and AuCu II′ ordered phases. Dark field TEM images (Figs. 10(a), 10(b) and 10(c)) suggest that these ordered phases are formed as platelets on {100} planes. Although the diffraction spots arising from the α_2' phase are indistinguishable in the SAED pattern, it can be deduced that the 200, 020, 220 and equivalent fundamental spots for the ordered phases coincide almost with the equivalent spots from the α_2' phase. As a result of further aging at 573 K, the diffraction spots from the α_2' phase became visible in SAED patterns.

3.5. Scanning electron microscopy observations

To clarify changes in microstructure corresponding to phase transformations, especially in a grain interior and at the grain boundary, SEM observations were made on specimens aged at 673, 623 and 573 K for various periods. For specimens aged at 673 K, a characteristic plate-like precipitate was observed in the interior of the grain after prolonged aging. A lamellar structure was also found primarily along grain boundaries, which later extruded into the interior of the grain.

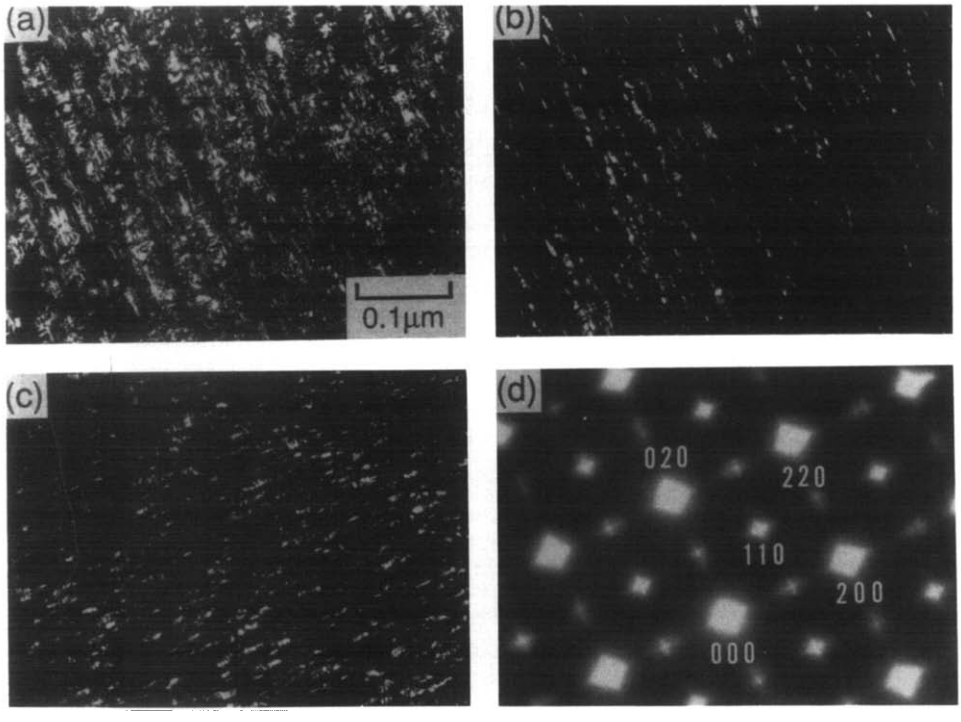

Fig. 10. TEM images and an SAED pattern taken for the specimen aged at 573 K for 1.8 ks: (a) the dark field image formed by using the 110 superlattice spot; (b), (c) dark field images formed by using the 001_X and 001_Y supperlattice spots respectively; (d) SAED pattern taken from the central area of the images.

The SEM micrographs of Fig. 11 demonstrate a growth of the lamellae by consumption of the interior of the grain caused by aging at 623 K. A Widmanstatten-like structure which suggests formation of networks of parallel platelets on certain lattice planes is observed in grains (Figs. 11(a) and 11(b)). After prolonged aging, the Widmanstatten structure changes into a different microstructure as seen in Fig. 11(c) or Fig. 11(d), which is an enlargement part of Fig. 11(c). It can be seen that the microstructure is composed of particles of cuboidal shape which are similar to etch pits. Therefore, it is suggested that these cuboidal particles correspond to the block-like α_2' region as indicated in the TEM micrographs and SAED pattern of Fig. 9.

Changes in the SEM microstructure after aging at 573 K are represented in Figs. 12(a), 12(b) and 12(c). The occurrence of twinning is observed at an early stage of aging, while the twin structure disappears and alternates to a stair–step arrangement of cuboidal blocks as seen in Fig. 12(d) which is an enlargement of part of Fig. 12(c) at a later stage of aging. From the XRD and TEM studies, it is expected that this stair–step structure consists

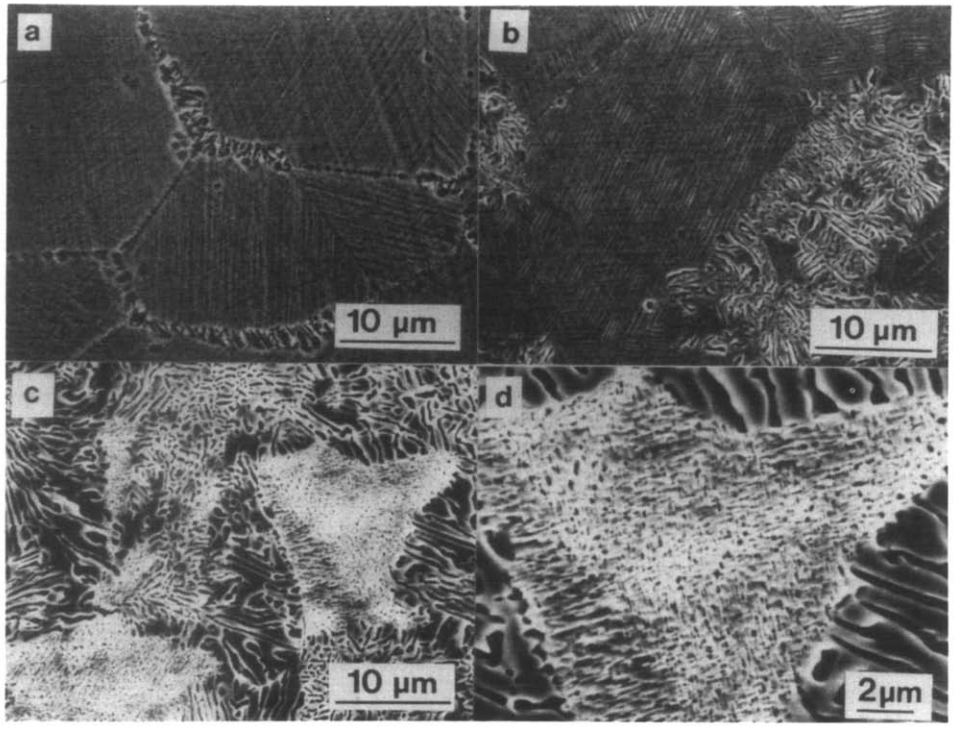

Fig. 11. Changes in SEM images caused by aging at 623 K for various periods: (a), (b), (c) aging periods of 60 ks, 1.8 Ms and 6 Ms respectively; (d) enlargement of part of (c).

of cuboidal block-like α_2' phases surrounding the matrix AuCu I′ and AuCu II′ ordered phases. Lamellar precipitates are also found at the grain boundary.

4. Discussion

Table 1 summarizes the results obtained in the present study. Notwithstanding that discrepancies in sensitivity to heat treatment actually exist because of time lags due to differences in the sizes of the specimens among the experimental methods, the results exhibit good agreement for critical temperatures, coexisting phases in each temperature range, and microstructures. TEM and SAED studies make it possible to detect phase transformations occurring in the interior of grains depending on microstructure and crystal structure. SEM observations reveal grain boundary precipitation by a heterogeneous mechanism. On the contrary, XRD studies reveal a whole process of phase transformations occurring in the alloy, if the experiments are carried out by careful isothermal aging.

Thus, sequences of phase transformations in the present alloys at various temperatures are as follows.

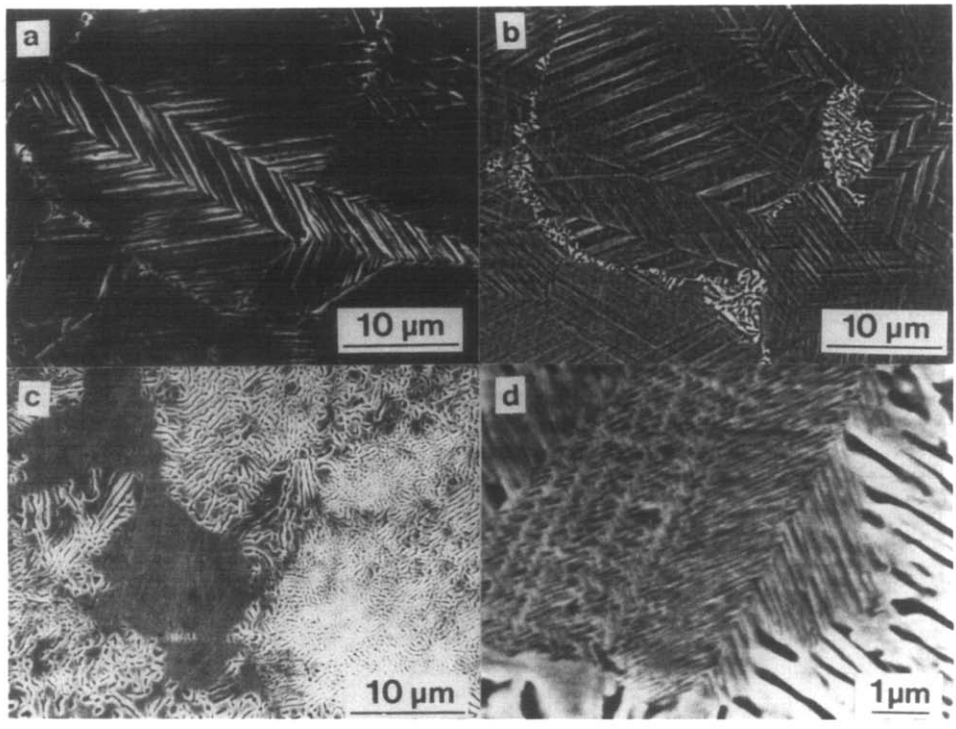

Fig. 12. Changes in SEM images caused by aging at 573 K for various periods: (a), (b), (c) aging periods of 60 ks, 600 ks and 18 Ms respectively; (d) enlargement of part of (c).

(1) At 673 K,

α_0 (f.c.c.) $\xrightarrow{\text{homogeneous}}$ α_1' (f.c.c.) + α_2' (f.c.c.) (within interior of the grain) $\xrightarrow{\text{heterogeneous}}$ α_1 (f.c.c.) + α_2 (f.c.c.) (at grain boundaries)

(2) At 623 K,

$\alpha_0 \xrightarrow{\text{homogeneous}}$ AuCu II′ (LPAPB ordered) + α_2' (within interior of the grain) → AuCu II′ + AuCu II + α_1 (f.c.c.) + α_2' + $\alpha_2 \xrightarrow{\text{heterogeneous}}$ AuCu II + α_1 + α_2 (at grain boundaries) where LPAPB denotes long period antiphase boundary.

(3) At 573 K,

$\alpha_0 \xrightarrow{\text{homogeneous}}$ AuCu I′ (f.c.t.) + AuCu II′ + α_2' (within interior of the grain) → AuCu I′ + AuCu I + AuCu II′ + AuCu II + α_2' + $\alpha_2 \xrightarrow{\text{heterogeneous}}$ AuCu I + AuCu II + α_2 (at grain boundaries)

(4) At 523 K,

$\alpha_0 \xrightarrow{\text{homogeneous}}$ AuCu I′ + α_2' (within interior of the grain) → AuCu I′ + AuCu I + α_2' + $\alpha_2 \xrightarrow{\text{heterogeneous}}$ AuCu I + α_2 (at grain boundaries)

Phases designated with a prime, *e.g.* AuCu II′, α_2', indicate metastable phases formed in the interior of grains; phases without a prime are equilibrium phases formed at grain boundaries. Age hardening in the alloy occurs depending

TABLE 1

Summary of the results obtained by various experimental methods

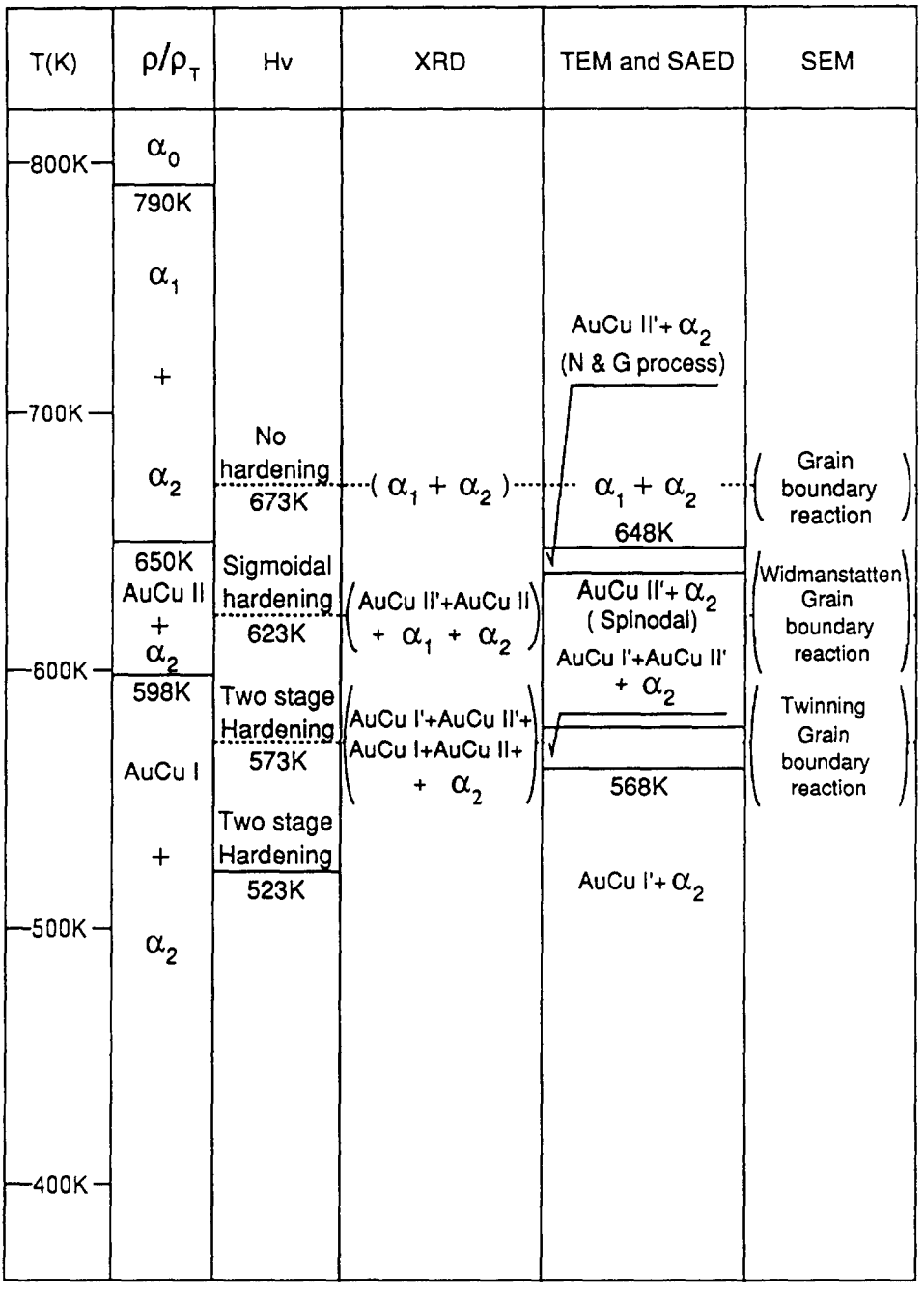

on the sequence of these phase transformations which itself depends on temperature.

In Fig. 2, there were two distinct hardening modes, *i.e.* a sigmoidal hardening curve obtained by aging at 623 K and a two-stage hardening curve obtained by aging below 573 K. It is thought that sigmoidal hardening is caused by a nucleation and growth process of phase transformations, *i.e.* formation of the AuCu II′ metastable LPAPB ordered phase. Although characteristic side-bands or satellite reflections arising from spinodal decomposition are not observed in XRD or SAED patterns during the early stage of aging at 623 K, it is expected that the spinodal locus is located at around 640 K, because TEM and SAED studies revealed that the growth rate of the AuCu II′ phase was considerably lower for aging at 643 K than at 633 K. Thus it is thought that ordering at 643 K is brought about by a nucleation and growth mechanism while ordering at 633 K is accelerated by the spinodal decomposition. Nevertheless, aging at 623 K exists just below the spinodal locus; a rapid increase in hardness is not observed (Fig. 2).

Miyazaki *et al.* [17] dealt with a theoretical analysis of two-phase decomposition derived from the Fourier expression of the non-linear diffusion equation on the basis of the Cahn–Hilliard flux equation. They presented composition profiles of a solute with continuing aging for various alloys which had a composition between the centre of the miscibility gap and just on the spinodal locus. Aging proceeded by a tendency to a nucleation and growth process during aging as was indicated by rectangularly shaped composition profiles. According to Miyazaki *et al.*, it was thought that hardening at 623 K was brought about by a nucleation and growth process of a two-phase decomposition accompanied by AuCu II′ ordering of the copper-rich metastable phase.

When aging was carried out below 573 K, the first hardening stage was induced by spinodal decomposition as was indicated by a rapid increase in hardness during the initial stage. The second hardening stage was attributed to strain induced by ordering of the metastable AuCu I′ and/or AuCu II′ phases depending on aging temperature. The drastic decrease in hardness at a later stage of aging coincides with the occurrence of grain boundary precipitates composed of AuCu I and/or AuCu II and the α_2 stable phases as was observed in SEM micrographs.

Acknowledgment

The authors gratefully acknowledge the financial support of the present study through the Japanese Ministry of Education, Science and Culture, Grant-in-Aid for Scientific Research (B) (01460241).

References

1 K. Yasuda and M. Ohta, *J. Less-Common. Met.*, *70* (1980) 75.
2 K. Hisatsune, M. Ohta, T. Shiraishi and M. Yamane, *J. Less-Common. Met.*, *83* (1982) 243.

3 K. Yasuda, K. Udoh, K. Hisatsune and M. Ohta, *Dent. Mater. J.*, *2* (1983) 48.
4 K. Udoh, K. Hisatsune, K. Yasuda and M. Ohta, *Dent. Mater. J.*, *3* (1984) 253.
5 K. Udoh, K. Yasuda and M. Ohta, *J. Less-Common. Met.*, *118* (1986) 249.
6 K. Yasuda, G. van Tendeloo, J. van Landuyt and S. Amelinckx, *J. Dent. Res.*, *65* (1986) 1179.
7 H. Yamauchi, H. A. Yoshimatsu, A. R. Forouhi and D. de Fontaine, *Proc. 4th Int. Precious Metals Conf., Toronto*, Pergamon, Oxford, 1980, p. 241.
8 T. Uzuka, Y. Kanzawa and K. Yasuda, *J. Dent. Res.*, *60* (1981) 883.
9 Y. Kanzawa, K. Yasuda and H. Metahi, *J. Less-Common. Met.*, *43* (1975) 121.
10 K. Yasuda, H. Metahi and Y. Kanzawa, *J. Less-Common. Met.*, *60* (1978) 65.
11 K. Yasuda and M. Ohta, *J. Dent. Res.*, *61* (1982) 473.
12 M. Ohta, T. Shiraishi, M. Yamane and K. Yasuda, *Dent. Mater. J.*, *2* (1983) 10.
13 M. Nakagawa and K. Yasuda, *J. Less-Common. Met.*, *138* (1988) 95.
14 K. Udoh, H. Fujiyama, K. Hisatsune, M. Hasaka and K. Yasuda, *J. Mater. Sci.*, in the press.
15 C. Johansson and J. Linde, *Ann. Phys.*, *25* (1936) 1.
16 K. Udoh, K. Yasuda, G. van Tendeloo and J. van Landuyt, *J. Alloys Comp.*, *176* (1991) 147–158.
17 T. Miyazaki, T. Kozaki, S. Mizuno and M. Doi, *Trans. Jpn. Inst. Met.*, *24* (1983) 246.